International Journal of Mass Spectrometry 312 (2012) 30–40

Contents lists available at SciVerse ScienceDirect

International Journal of Mass Spectrometry

journal homepage: www.elsevier.com/locate/ijms

Comparative profiling of the peroxisomal proteome of wildtype and *Pex7* knockout mice by quantitative mass spectrometry

Sebastian Wiese[a,1], Thomas Gronemeyer[b,1], Pedro Brites[c,e,1], Rob Ofman[c], Christian Bunse[d], Christian Renz[b], Helmut E. Meyer[d], Ronald J.A. Wanders[c], Bettina Warscheid[a,*]

[a] *Faculty of Biology and BIOSS Centre for Biological Signalling Studies, University of Freiburg, 79104 Freiburg, Germany*
[b] *Department of Molecular Genetics and Cell Biology, Ulm University, 89081 Ulm, Germany*
[c] *Laboratory of Genetic Metabolic Diseases, Department of Clinical Chemistry and Pediatrics, Academic Medical Center, University of Amsterdam, P.O. Box 22700, 1100 DE, Amsterdam, The Netherlands*
[d] *Medizinisches Proteom-Center, Ruhr-Universitaet Bochum, 44780 Bochum, Germany*
[e] *Nerve Regeneration Group, Institute for Molecular and Cell Biology, 4150-180 Porto, Portugal*

ARTICLE INFO

Article history:
Received 7 June 2011
Received in revised form 7 September 2011
Accepted 8 September 2011
Available online 2 October 2011

Keywords:
Quantitative mass spectrometry
Label-free protein profiling
Organellar proteomics
Peroxisomes
Peroxisomal targeting signal 2
Mouse kidney

ABSTRACT

We present a label-free quantitative proteomic approach for the study of kidney peroxisomes of *Pex7* knockout mice which is a *bona-fide* model for the human disease rhizomelic chondrodysplasia punctata (RCDP). RCDP is an autosomal recessive human disorder caused by mutations in the *PEX7* gene encoding for Pex7, the cytosolic receptor protein that is essential for the import of proteins containing a functional peroxisomal targeting signal (PTS)-type 2. In this work, we quantitatively followed hundreds of proteins through high density gradient fractions of wildtype (WT) and *Pex7* knockout (*Pex7*$^{-/-}$) mice by high resolution mass spectrometry. A set of candidate proteins with altered abundance was defined via statistical and quantitative assessment of protein profiles obtained from WT and *Pex7*$^{-/-}$ mice. The results obtained demonstrate the feasibility of this approach to identify proteins specifically affected in abundance by the deletion of Pex7. All three known PTS2 proteins, including acetyl-Coenzyme A acyltransferase, alkylglycerone phosphate synthase and phytanoyl-CoA hydroxylase were determined to be virtually absent in these fractions whereas KIAA0564, a so far uncharacterized protein, was barely detectable in peroxisomal fractions of *Pex7*$^{-/-}$ mice. Furthermore, we report numerous PTS1 proteins with increased abundance levels in *Pex7*$^{-/-}$ mice that fulfill essential functions in the β-oxidation of very long-chain fatty acids or the biosynthesis of ether-phospholipids in peroxisomes.

1. Introduction

The combination of classical subcellular fractionation techniques and modern mass spectrometry (MS) provides a powerful tool for characterizing the protein inventory of organelles in eukaryotic cells. Such membrane-bound cellular compartments serve as defined microenvironments allowing proteins to fulfill their specific functions. Detailed knowledge about the subcellular localization of proteins is therefore a prerequisite to elucidate the spatial distribution of complex metabolic pathways and intricate protein signaling networks. So far, application of MS-based proteomics approaches has already allowed for gathering extensive information about various organellar proteomes from different organisms [1–6]. However, major challenges in organellar proteomics endeavors still remain. First, organelles cannot be purified to homogeneity leading to a large background of low abundant co-purified contaminants readily detected when the latest LC/MS technologies are used. Secondly, isolation of low abundant and highly dynamic organelles such as peroxisomes from different tissues remains difficult [7]. And thirdly, identification of new organellar resident proteins requires the development of comprehensive strategies preferably using quantitative MS for reliably identifying candidate proteins followed, for example, by imaging approaches for *in vivo* co-localization studies to validate the MS data.

In recent years, interest in the functional characterization of peroxisomes has been fueled by the existence of severe inherited diseases in humans, classified into peroxisomal biogenesis disorders (PBDs) and single peroxisomal enzyme deficiencies, that are caused by the malfunctioning of this organelle [8–10]. Mutations in at least 12 different genes encoding for proteins essential for

Abbreviations: CoA, Coenzyme A; IPI, international protein index; OBCOL, organelle based colocalisation; PTS, peroxisomal targeting signal; PBD, peroxisomal biogenesis disorder; RCDP, rhizomelic chondrodysplasia punctata; VLCFA, very long-chain fatty acid.

* Corresponding author. Tel.: +49 761 203 2690; fax: +49 761 203 2601.
E-mail address: Bettina.Warscheid@biologie.uni-freiburg.de (B. Warscheid).

[1] These authors contributed equally to this work.

1387-3806/$ – see front matter © 2011 Elsevier B.V. All rights reserved.
doi:10.1016/j.ijms.2011.09.005

the biogenesis of fully functional peroxisomes (the so-called peroxins) have been identified, which constitute the group of PBDs. Among these, mutations in the *PEX7* gene encoding for the cytosolic receptor protein Pex7 cause rhizomelic chondrodysplasia punctata (RCDP) type 1, an autosomal recessive human disorder characterized by skeletal, facial, eye and brain abnormalities as well as growth deficiencies [11–14].

Pex7 is one of two receptors for peroxisomal matrix proteins synthesized at free ribosomes in the cytosol [15–18]. To execute their distinct metabolic functions such as α- and β-oxidation of fatty acids, plasmalogen biosynthesis or detoxification of glyoxylate, peroxisomal enzymes have to be post-translationally imported into peroxisomes [19,20]. Most of these proteins contain the conserved C-terminal targeting sequence (S/A/C)(K/R/H)L, termed peroxisomal targeting signal (PTS) type 1, and are recognized by their cognate receptor Pex5 [21,22]. However, a few enzymes containing the sequence (R/K)(L/V/I)X_5(H/Q)(L/A) typically located in the N-terminal region (termed PTS2) are recognized by Pex7 [18,23–25]. In mammals, import of proteins via the PTS2 pathway further requires binding of Pex7 to its co-receptor Pex5pL, a long splice isoform of Pex5 that facilitates targeting of Pex7-cargo complexes to peroxisomes [26–28]. So far, more than 20 different mutations in the *PEX7* gene have been identified in RCDP type 1 patients [29–31]. As a consequence, the import of the mammalian PTS2 proteins acetyl-Coenzyme A (CoA) acyltransferase (Acaa1)[32], alkylglycerone phosphate synthase (Agps)[33], and phytanoyl-CoA hydroxylase (Phyh) [34–36] is abolished. Impaired import of Phyh and Agps leads to the accumulation of phytanic acid [37] and deficient synthesis of plasmalogens [38,39], respectively. Interestingly, deficient import of Acaa1 did not affect fatty acid β-oxidation in RCDP type 1 patients [14,40,41]. Despite extensive research, the existence of further enzymes imported into peroxisomes via the Pex7 pathway and, thus, potentially involved in RCDP type 1 is still a matter of debate. To address this question, MS-based organellar proteomics provides a promising path to follow. For a comprehensive analysis of mammalian peroxisomes, their functional diversity accompanied by characteristic differences in their proteomes needs to be taken into account [42], which highlights the importance of tissue-specific proteomics studies of mammalian peroxisomes. Previous gel-based and gel-enhanced studies of rat liver and mouse kidney peroxisomes has led to the identification of approx. 50 membrane and matrix proteins including three new peroxisomal enzymes [43–45]. Recently, the number of peroxisomal proteins was further boosted by approx. one-third through the application of quantitative MS [46,47] assisting in the establishment of the protein inventory of mammalian peroxisomes as summarized in the peroxisome database (http://www.peroxisomedb.org/; [48]). However, while these approaches allowed to identify several new peroxisomal proteins containing a putative PTS1 (e.g., Zadh2, Acad11, Tysnd1, RP2), they failed in the discovery of new PTS2 candidate proteins.

In this work, a label-free quantitative MS-based protein profiling approach to comparatively study kidney peroxisomes of wildtype (WT) and *Pex7* knockout (*Pex7*$^{-/-}$) mice was established. Abundance profiles of hundreds of proteins were generated based on the analysis of Nycodenz density gradient fractions of WT and *Pex7*$^{-/-}$ mice by high resolution MS combined with MaxQuant data processing. In order to identify proteins specifically affected in abundance by the deletion of Pex7, a set of peroxisomal candidate proteins was defined via statistics. Among the identified proteins that were barely detectable in peroxisome-enriched fractions of *Pex7*$^{-/-}$ mice were all known PTS2 proteins (Acaa1, Agps, Phyh) and KIAA0564, a so far uncharacterized protein. Moreover, we found considerably increased abundance levels of numerous peroxisomal PTS1 proteins in *Pex7*$^{-/-}$ mice and based on co-localization studies we provide a first cue for KIAA0564 being possibly imported into peroxisomes.

2. Materials and methods

2.1. Peroxisome preparations

Peroxisomes were purified from kidneys of female Swiss WT and *Pex7*$^{-/-}$ mice [49] as described previously [45]. In brief, kidneys were homogenized in a buffer consisting of 10 mM morpholinopropanesulphonic acid–NaOH, 250 mM sucrose, 2 mM EDTA, and 0.1% ethanol (final pH 7.4). A postnuclear supernatant was prepared by centrifugation of the homogenate for 10 min at 600 *g* and 4 °C. Peroxisomes from WT and *Pex7*$^{-/-}$ mice were then isolated separately by Nycodenz equilibrium density gradient centrifugation as described before [50]. For mass spectrometric analyses, organellar pellets were prepared by centrifugation (16,000 *g* and 4 °C for 10 min) from 1-ml aliquots of high density fractions of the *Pex7*$^{-/-}$ and the WT gradient and stored at −80 °C. Prior to use, proteins were resuspended in sample buffer containing 30 mM Tris–HCl, 2 M thiourea, and 7 M urea (pH 8.5) to reach a final protein concentration of about 1 μg/μl. For improved protein identification and reliable protein quantification, each gradient fraction was analyzed in triplicates.

2.2. Proteolytic digestion

Protein samples were diluted in 50 mM NH_4HCO_3 (pH 7.8) to reach a final protein concentration of 0.1 μg/μl. Trypsin (Promega, Madison, USA) was added at a protein-to-trypsin ratio of 1:30 and enzymatic digestion was carried out for 6 h at 37 °C. For mass spectrometric analyses, all samples were processed in parallel and peptide mixtures were diluted in 5% formic acid to reach a concentration of 0.067 μg/μl.

2.3. Mass spectrometry

Online reversed-phase capillary HPLC separations were performed using the UltiMate™ 3000 HPLC system (Dionex LC Packings, Idstein, Germany) as described previously [51]. Electrospray ionization tandem mass spectrometry (ESI-MS/MS) was performed on an LTQ Orbitrap XL instrument (Thermo Fisher Scientific, Bremen, Germany) equipped with a nanoelectrospray ion source. Tryptic peptide mixtures from density gradient fractions of WT and *Pex7*$^{-/-}$ mice were consecutively analyzed in random order employing the same LC/MS system. Blanks were run routinely and the performance of the system was checked daily by analyzing a standard peptide mixture. For MS and MS/MS analyses, the instrument was operated in the data-dependent mode. Survey MS spectra from *m*/*z* 300 to 2000 were acquired in the Orbitrap with $r = 60{,}000$ at *m*/*z* 400 and a target accumulation value of 500,000. The six most intense multiply charged peptide ions were sequentially selected for fragmentation in the linear ion trap by low-energy CID (target accumulation value of 10,000). Former target ions selected for MS/MS were dynamically excluded for 45 s. The parent mass accuracy was set to 20 ppm. Further general mass spectrometric parameters were as follows: spray voltage, 1.7 kV; ion transfer tube temperature, 200 °C; normalized collision energy of 35% for MS/MS with an activation $q = 0.25$ and an activation time of 30 ms. The ion selection threshold was set to 500 counts.

2.4. Mass spectrometric data analysis

Mass spectrometric data were processed using the software MaxQuant (version 1.1.1.25). For peptide and protein identification,

data were correlated with the mouse International Protein Index (Mouse IPI V3.68; www.ebi.ac.uk) database containing 56,743 protein entries using Andromeda [52]. All searches were performed with tryptic specificity allowing two missed cleavages. Oxidation of methionine and acetylation of protein N-termini were considered as variable modifications. No fixed modifications were considered. Raw data were recalibrated using the "first search" option of Andromeda with a database containing a subset of abundant mouse proteins. Mass spectra were searched using the default settings of Andromeda. A false discovery rate of 1% was applied on both peptide and protein level. In the experimental design template, triplicate measurements of gradient fractions were combined to a single experiment.

2.5. Protein profiles and statistics

For the generation of protein profiles, signals of corresponding peptides in different nano-HPLC/ESI-MS/MS runs were matched by MaxQuant applying a mass accuracy of at least 20 ppm and a maximum time window of 4 min. Protein profiles are based on the signal intensities of all peptides assigned to a given protein in each of the fractions analyzed. For statistical analysis, the resulting protein profiles for the WT and *Pex7*$^{-/-}$ gradient were normalized to the fraction with the highest intensity. The mean profiles of a total of 83 and 84 proteins assigned to peroxisomes according to the protein knowledgebase UniProtKB (http://www.uniprot.org/) were calculated for the WT and *Pex7*$^{-/-}$ gradient, respectively. Next, the Euclidian distance (*P*) between these two mean profiles and all individual protein profiles were calculated for fractions 1–4 and 1–5 for the WT and the *Pex7*$^{-/-}$ gradient, respectively. Proteins were sorted according to their *P*-values. All proteins up to sensitivities of 80% in WT and 70% in *Pex7*$^{-/-}$, which is equivalent to a P^{WT}-value of 0.18 and a $P^{Pex7-/-}$-value of 0.17, that were reliably identified with more than 5 peptides were considered for further analysis. Of these, proteins with a P^{WT}-value below 0.18 and an accumulated intensity in all *Pex7*$^{-/-}$ gradient fractions of less than 20% of the accumulated WT intensities were considered to be likely imported into peroxisomes via Pex7. Correspondingly, proteins reliably identified in the WT gradient and with both a $P^{Pex7-/-}$-value below 0.17 and an accumulated intensity of less than 2.5% of the accumulated Pex7$^{-/-}$ intensities were additionally considered to be affected by the deletion of Pex7.

2.6. Cloning of KIAA0564 fragments, cell culture, and fluorescence microscopy

A fragment of KIAA0564 (corresponding to amino acids 478–939) containing both predicted ATPases Associated with diverse cellular activities (AAA) domains and a putative PTS2 was amplified from the KIAA0564 cDNA clone (commercially available from Imagenes GmbH, Berlin, Germany) using PCR standard techniques. A Kozak sequence and the sequence coding for the hemagglutinin (HA) affinity tag were introduced upstream of the open reading frame. The sequence was subsequently cloned into the eukaryotic expression vector pDsRed-C1-monomer (BD Biosciences/Clontech, Heidelberg, Germany) via the *Nhe1 and Age1* restriction sites resulting in expression of a HA-KIAA0564(478–939)-DsRed fusion protein. An L789S point mutation within the PTS2 was introduced into HA-KIAA0564(478–939)-DsRed by overlapping PCR. To test for potential import of KIAA0564 into the peroxisomes by piggyback transport, a cDNA fragment corresponding to amino acids 764–833 and containing the predicted PTS2 was cloned into pDsRed-C1-monomer as outlined above. A list of all PCR primers is available upon request.

Huh7 cells were cultivated in Dulbecco's modified Eagle's medium (Gibco/Invitrogen, Karlsruhe, Germany) supplemented with 10% fetal calf serum (Gibco/Invitrogen) at 37 °C (5% CO_2). Transfection with KIAA0564 expression constructs was performed using the calcium phosphate method. After 24 h, cells were subjected to 500 mg/l Geneticin (Gibco/Invitrogen) to select for stable KIAA0564(478–939) and KIAA0564(478–939)L789S transfectants and finally maintained in medium containing 250 mg/l Geneticin. For immunofluorescence, stably transfected cells were grown on glass cover slips for 24 h, fixed in 3% paraformaldehyde (PFA) and permeabilized with 1% Triton X-100 for 5 min. After blocking with 10% BSA, cells were incubated with a mixture of a guinea pig anti-catalase (kind gift of Wilhelm Just, Heidelberg, Germany) and a mouse anti-HA antibody (Sigma, Taufkirchen, Germany), both diluted 1:250 in 1% BSA, for 1 h at 37 °C. Cells were then incubated for 1 h at 37 °C with secondary antibodies (Alexa-488 anti-mouse and Alexa-547 anti-guinea pig; Invitrogen, Karlsruhe, Germany) diluted 1:500 in 1% BSA. Furthermore, Huh7 cells grown on coverslips were transiently cotransfected with the HA-KIAA0564(764–833)-DsRed construct and pEGFP-peroxi, a plasmid leading to the expression of GFP-SKL as a peroxisomal marker (BD Biosciences/Clontech, Heidelberg, Germany). Transiently transfected cells were grown for further 48 h and fixed with 3% PFA. Cover slips were eventually mounted onto microscope slides using VectaShield hard set mounting medium (Vector Laboratories, Burlingame, CA).

Microscopy was carried out using an Axio Oberserver SD confocal microscope (Zeiss, Göttingen, Germany) equipped with 488 nm and 547 nm diode lasers and a Plan-Apochromat 63× (lens aperture 1.4) objective. Image acquisition and primary processing was performed using the Zeiss AxioVision software (version 4.8.1). Prior to quantification of co-localizing structures, *z*-stacks (usually 5–10 *z*-layers per stack depending on the specimen) were filtered using the Gauss filter implemented in the image acquisition software to remove noise. Stacks were subsequently exported separately for the 488 and 547 nm channel as 8-bit greyscale images in tif-format and the analysis was performed using ImageJ (http://rsb.info.nih.gov/ij/) and the OBCOL plugin [53]. Parameters were set to default of the OBCOL pipeline as described [53]. A Pearson's coefficient of ≥0.5 indicated co-localization of subcellular structures from the 488 and 547 nm channel, respectively. Counting of the total number of peroxisomes present in the stack was performed with the "3D object counter" plugin implemented in ImageJ.

3. Results

We combined density gradient centrifugation with label-free, quantitative MS to differentially analyze the proteome of kidney peroxisomes from WT and *Pex7*$^{-/-}$ mice aiming at the identification of proteins that are specifically affected by the deletion of Pex7. We anticipated that PTS1-containing proteins can be readily detected in peroxisomes of both WT and *Pex7*$^{-/-}$ mice. In contrast, proteins imported via the Pex7 pathway were expected to be unambiguously identified in WT peroxisomes but barely detectable in peroxisomes of *Pex7*$^{-/-}$ mice. We prepared peroxisomes from kidneys of WT and *Pex7*$^{-/-}$ mice by differential and Nycodenz density gradient centrifugation according to Ofman et al. [45]. Since peroxisomes from mouse kidneys are enriched in high density fractions [45,47], we collected 5 consecutive fractions of 2 ml from the bottom of each gradient. Following the preparation of organellar pellets, proteins in WT and *Pex7*$^{-/-}$ gradient fractions were tryptically digested and the resulting peptide mixtures were randomly analyzed in triplicates by nano-HPLC/ESI-MS/MS on an LTQ-Orbitrap instrument. Total ion and base peak chromatograms

Table 1
Overview of proteins and their subcellular localization identified in high density fractions of kidneys from wildtype (WT) and *Pex7* knockout (*Pex7*$^{-/-}$) mice. Numbers in parenthesis indicate the abundance (in percent) of each protein group based on the measured signal intensities in MS1 scans. Mean peroxisomal profiles were calculated based on the normalized abundance of all peroxisomal proteins according to information in the UniProt protein knowledgebase (www.uniprot.org; for detailed information on the calculation of mean profiles refer to Section 2).

Number of (abundance, %)	WT				*Pex7*$^{-/-}$					Total
	1	2	3	4	1	2	3	4	5	
All identified proteins	187	587	672	576	662	548	576	786	833	985
Peroxisomal proteins	53 (11.1)	71 (43.5)	80 (81.9)	70 (36.5)	78 (57.5)	76 (75.0)	81 (91.7)	82 (78.2)	79 (51.3)	86 (71.0)
[5pt] Mitochondrial proteins	28 (0.3)	173 (15.1)	192 (4.0)	184 (17.3)	204 (11.3)	175 (3.8)	162 (1.2)	241 (10.0)	242 (23.6)	265 (7.0)
Cytoplasmic proteins	49 (73.0)	118 (17.5)	130 (4.5)	105 (10.5)	130 (14.2)	99 (8.3)	127 (2.6)	153 (4.3)	158 (10.5)	197 (11.9)
Proteins from other organelles	38 (10.2)	168 (15.0)	206 (7.8)	165 (27.5)	188 (11.8)	146 (8.3)	150 (3.7)	234 (6.3)	275 (12.9)	333 (8.5)
Proteins with unknown localization	19 (5.4)	57 (9.0)	64 (1.7)	52 (5.3)	104 (5.3)	62 (4.6)	52 (1.0)	56 (1.2)	76 (1.8)	104 (1.7)
Mean peroxisomal profile	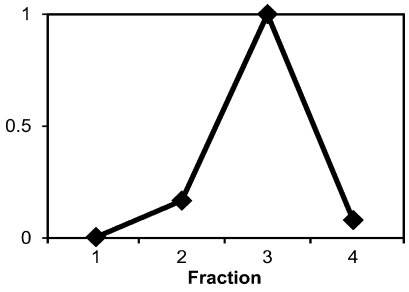				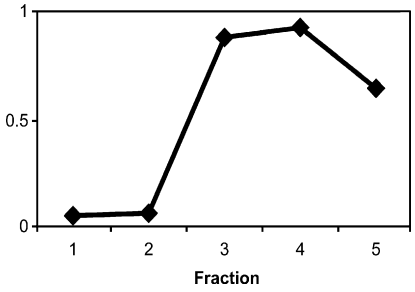					

were consistent between LC/MS analyses of all fractions except for all replicates of fraction 5 of the WT gradient in which we detected considerably higher signal intensities (data not shown). Arguably, the latter observation may result from intrinsic variation(s) in sample fractionation and/or processing. However, since peroxisomal proteins exhibited a distinct maximum in fraction 3 of the WT gradient, we focused on fractions 1–4 of the WT gradient in our further analyses to delineate the distribution profile of PTS1 and PTS2 proteins.

Table 1 summarizes all protein identification data obtained from high density fractions of WT (fraction 1–4) and *Pex7*$^{-/-}$ (fraction 1–5) gradients obtained via LC/MS and MaxQuant analyses. Combined evaluation of MS/MS data from both WT and *Pex7*$^{-/-}$ gradient fractions led to the identification of a total of 985 non-redundant proteins or protein groups with a false discovery rate of 1% (for detailed information about protein and peptide identification results, refer to Supplementary Tables 1A and 1C). For individual fractions, the number of proteins identified was mainly in the range of 540–830. The overlaps between proteins identified in the fractions 2–4 of the WT and *Pex7*$^{-/-}$ gradient were in the range of 65–68%, indicating a high consistency of the data acquired. LC/MS analyses performed in this work resulted in the identification of 86 peroxisomal proteins and protein isoforms according to the current information provided by the protein knowledgebase UniProtKB (http://www.uniprot.org/) (Supplementary Table 1A). Of these, 78 (59 matrix and 19 membrane proteins) are listed in the peroxisome database (www.peroxisomedb.org) to date. Notably, we achieved an average overlap of 85% for peroxisomal proteins identified in fractions 2–4 of WT and *Pex7*$^{-/-}$ gradients and identified virtually all peroxisomal matrix components involved in the different metabolic pathways such as the β-oxidation of VLCFAs, the α-oxidation of phytanic acid, the synthesis of plasmalogens as well as the metabolism of amino acids and reactive oxygen species (Supplementary Table 1A and 1B). Peroxisomal proteins exclusively identified in the WT were the PTS1 protein bile acid-CoA:amino acid N-acyltransferase and the PTS2 protein Agps, whereas two low abundant peroxisomal membrane proteins, Pex2 and Mpv17 protein, were identified in *Pex7*$^{-/-}$ mice only. Supplementary Table 1B provides a compilation of all the peroxisomal proteins identified in this work according to the peroxisome database (www.peroxisomedb.org) and further includes current knowledge about the proteome of mammalian peroxisomes including information on gene names, accession numbers, general functions as well as reported PTS1- and PTS2-sequences in peroxisomal matrix proteins. We covered 72% of all the proteins reported to be associated with mammalian peroxisomes not accounting for differences in the peroxisomal proteomes of different tissues and organisms (Supplementary Table 1B). However, due to (i) the fact that peroxisomes cannot be purified to homogeneity and (ii) the high sensitivity of LC/MS analyses performed in this work, a high number of co-purifying proteins mainly originating from the cytoplasm (197 proteins), mitochondria (265 proteins) and other organelles (333 proteins) as well as proteins of unknown localization (104) were identified as well. Although these proteins contributed to more than 90% of all identifications, their overall relative abundance calculated on the basis of the sum of all peptide intensities was less than 30% (Table 1, Supplementary Table 1A). In fact, the sum of all peptide intensities assigned to known peroxisomal proteins (9% of all protein identifications) was 82% and 92% of the total peptide intensity measured in fraction 3 of the WT and *Pex7*$^{-/-}$ gradient, respectively. These data clearly indicate that the pool of non-peroxisomal proteins represents co-purifying contaminants of very low abundance in our analysis. Taken together, we were able to compile a most comprehensive protein inventory of kidney peroxisomes from both WT and *Pex7*$^{-/-}$ mice suitable for further quantitative examination.

3.1. Identification of peroxisomal proteins affected by the deletion of Pex7

For a thorough comparative analysis of the proteomes of kidney peroxisomes from WT and *Pex7*$^{-/-}$ mice, we quantitatively followed proteins through several high density fractions and established the respective abundance distributions (Supplementary Table 1A). We then calculated the mean peroxisomal profiles based on the normalized abundance of all peroxisomal proteins identified in high density fractions from WT and *Pex7*$^{-/-}$ gradients, thereby establishing a reference profile for assigning proteins to peroxisomes. Interestingly, WT peroxisomes showed a narrow distribution peaking in fraction 3, whereas *Pex7*$^{-/-}$ peroxisomes exhibited a slightly broader distribution with highest abundances in fraction 3 and 4 (Table 1). Furthermore, the relative abundance of peroxisomal proteins was on average 10% higher in fractions from the *Pex7*$^{-/-}$ compared to fractions from the WT gradient (Supplementary Table 1A). Next, the Euclidian distance (P) values between the WT and the *Pex7*$^{-/-}$ mean peroxisomal profile and all individual protein profiles were calculated in order to distinguish between proteins specifically associated with peroxisomes and co-purifying contaminants (Supplementary Table 1A). For comparative analysis, we only considered proteins with more than five peptide identifications and a P^{WT}- or $P^{Pex7-/-}$-value below 0.18 and 0.17.

Fig. 1A exemplarily depicts the abundance profiles of acyl-CoA oxidase 2 (Acox2) and 2-4-dienoyl-CoA reductase 2 (Decr2), two enzymes involved in peroxisomal fatty acid β-oxidation. Both proteins contain a functional PTS1 and are imported into peroxisomes via Pex5. Correspondingly, the protein profiles resemble well the mean peroxisomal profile in the WT and *Pex7*$^{-/-}$ gradient (Table 1 and Supplementary Table 1A). In contrast, Phyh, Agps, Acaa1 isoforms a and b as well as KIAA0564 showed a peroxisome-characteristic profile in the WT, whereas they were virtually absent or strongly reduced in intensity in the *Pex7*$^{-/-}$ gradient (Fig. 1B, Supplementary Table 1A). Based on this observation we conclude that these proteins, among which are all the currently known peroxisomal enzymes containing a functional PTS2, are transported from the cytosol into peroxisomes via the Pex7 import pathway. Furthermore, the data demonstrate the feasibility of our quantitative MS approach to identify proteins specifically affected by the deletion of Pex7. Apart from the three known PTS2 proteins, KIAA0564 showed a more than 5-fold decrease of total intensity measured in *Pex7*$^{-/-}$ compared to WT fractions and, hence, was considered a new candidate protein following the Pex7 import pathway.

Interestingly, we identified several peroxisomal enzymes involved in β-oxidation of VLCFAs and plasmalogen biosynthesis, that were considerably more abundant in *Pex7*$^{-/-}$ compared to WT fractions. These proteins were fatty acyl CoA reductase 1 (Far1) isoform 4, serine hydrolase-like protein (Serhl), lon protease-like protein 2 (Lonp2), and long-chain acyl-CoA synthetase 1 (Acsl1), all exhibiting a more than 40-fold higher abundance in *Pex7*$^{-/-}$ compared to WT fractions (Fig. 2, Supplementary Table 1A). Further enzymes known to be part of these metabolic pathways and found to be of higher abundance in *Pex7*$^{-/-}$ mice were acyl-CoA oxidase 1 (Acox1), 17-beta-hydroxysteroid dehydrogenase 4 (Edh17b4), the acyl-CoA thioesterases Acot3, Acot6 and Acot8 as well as the sterol-carrier protein 2 (Scp2) (Supplementary Table 1A).

3.2. Analysis of KIAA0564 fragments by fluorescence microscopy

Comparative protein profiling led to the identification of mouse KIAA0564, a protein of so far unknown function and localization, as new putative candidate protein associated with the Pex7 import receptor. In follow up studies, we used the human hepatocellular carcinoma cell line Huh7 expressing fusion proteins of the human homologue of the mouse KIAA0564 protein (sequence identity 86%) and fluorescence microscopy for colocalization studies. The human KIAA0564 protein comprises 1905 amino acids and, consistent with its mouse homologue, contains a putative PTS2 (KIVDRFLHL at aa 781–789) as predicted using PSORT [54]. BLAST alignment of the amino acid sequence indicated two putative AAA domains (aa 615–739 and aa 773–905) and a putative Van Willebrand domain (aa 1712–1901) at the very C-terminus of the protein. For microscopic analysis, we used a fragment of KIAA0564 (corresponding to amino acids 478–939) containing the putative PTS2 [KIAA0564(478–939)]. We further investigated whether the L789S point mutation in the predicted PTS2 sequence [KIAA0564(478–939)-L789S] affects the association of the KIAA0564(478–939) fragment with peroxisomes. Both fragments carried an N-terminal HA tag and the red fluorescent protein DsRed at the C-terminus. In a first experiment, Huh7 cells were transiently cotransfected with the HA-KIAA0564(478–939)-DsRed fusion construct and the peroxisomal marker GFP-SKL. We observed a punctate pattern for GFP-SKL indicative for peroxisomes; however, no signal for the DsRed fusion protein was detected pointing to a weak expression and/or low copy numbers per cell (data not shown).

To further study the peroxisomal localization of the KIAA0564 fragments, we generated Huh7 cell lines stably expressing one of the two constructs. We used anti-HA and anti-catalase antibodies to detect the KIAA0564 fusion proteins and peroxisomes by immunofluorescence microscopy. As shown in Fig. 3, a punctate pattern was observed for both KIAA0564(478–939) (Fig. 3A) and KIAA0564(478–939)-L789S (Fig. 3B) which corresponds well to the pattern of the peroxisomal marker protein catalase. Interestingly, the total average number of peroxisomes was lower in Huh7 cells expressing the KIAA0564(478–939)-L789S fragment (126 ± 15, $n = 80$) compared to cells expressing the WT fragment (189 ± 14, $n = 71$) (Fig. 3C). To determine the degree of punctate substructures showing colocalization, we performed organelle-based colocalization (OBCOL) analysis [53]. In cells stably transfected with KIAA0564(478–939) and KIAA0564(478–939)-L789S, the number of colocalizing substructures was 106 ± 17 ($n = 71$) and 61 ± 11 ($n = 80$), respectively (Fig. 3D). Taken together, we found a significant 33% decrease in peroxisome number, while the number of colocalizing substructures was only slightly decreased from 56% to 48% in cells expressing KIAA0564(478–939)-L789S compared to cells expressing the WT fragment.

In mammals, Cu/Zn superoxide dismutase was recently reported to form a complex with the PTS1-containing protein copper chaperone of SOD1 allowing it to get into peroxisomes via piggy-back transport [55]. To investigate whether KIAA0564(478–939) fusion proteins follow a classical PTS-dependent import route, we cloned a short, the PTS2 containing fragment of 69 amino acids (764–833) as DsRed fusion construct [KIAA0564(764–833)] and used GFP-SKL as peroxisomal marker for colocalization studies by fluorescence microscopy. While we observed cytosolic expression of the construct in a few single cells (data not shown), almost exclusive colocalization of the short KIAA0564(764–833) fragment with peroxisomes was found in the majority of the cells (Fig. 4).

4. Discussion

We subjected postnuclear supernatants of kidneys from WT and *Pex7*$^{-/-}$ mice to differential and Nycodenz density gradient centrifugation and analyzed the resulting high density fractions by label-free quantitative MS. Proteomic analysis of mouse kidney peroxisomes using a high resolution LTQ-Orbitrap instrument and MaxQuant provided high sensitivity for identification and

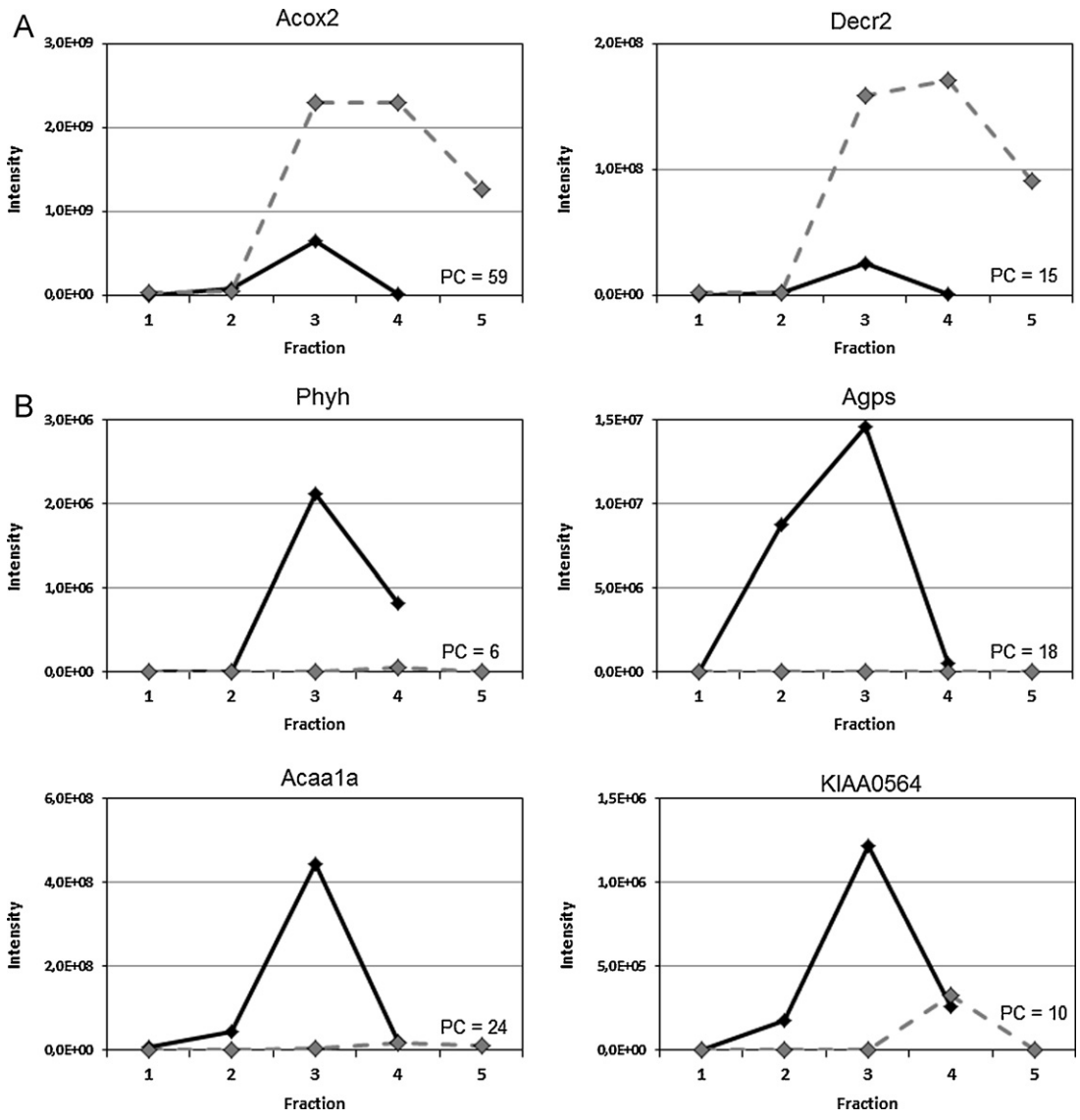

Fig. 1. Comparative protein profiling of high density fractions of kidneys from wildtype (WT, bold line) and Pex7 knockout (*Pex7*$^{-/-}$, dashed line) mice. (A) Intensity profiles of acyl-Coenzyme A oxidase 2 (Acox2) and 2-4-dienoyl-Coenzyme A reductase 2 (Dcr2) in WT and *Pex7*$^{-/-}$ fractions. Both proteins carry a peroxisomal targeting signal (PTS) type 1 and are imported via the receptor protein Pex5 into peroxisomes. (B) Intensity profiles of phytanoyl-Coenzyme A hydroxylase (Phyh), alkylglycerone phosphate synthase (Agps), acetyl-Coenzyme A acyltransferase Acaa1 isoform a and KIAA0564 in WT and *Pex7*$^{-/-}$ fractions. The first three proteins are known functional PTS2-containing proteins, whereas KIAA0564 represents a new candidate protein potentially imported via Pex7 into peroxisomes. PC, peptide count.

label-free protein quantification allowing us to report here 86 peroxisomal proteins and protein isoforms, of which 78 are currently listed in the peroxisome database (www.peroxisomedb.org) (Supplementary Table 1B). We could consistently detect virtually all enzymes essential for peroxisomal fatty acid α- and β-oxidation, plasmalogen synthesis, amino acid metabolism and reactive oxygen species degradation in high density fractions of both WT and *Pex7*$^{-/-}$ mice. Except for Pex26 as well as Pex7 and Pex19, two shuttling receptors mainly located in the cytosol [18,56], all membrane-associated proteins essential for the biogenesis and proliferation of peroxisomes were detected. Furthermore, our data confirmed the presence of virtually all new constituents reported recently for liver [44,46] and kidney [45,47] peroxisomes, such as Pmp52, Acad11, Mosc2, Acbd5, Atad1, Tysnd1, Zadh2, and Nudt19. Thus, we could compile a virtually complete and consistent protein inventory of peroxisomes from both WT and *Pex7*$^{-/-}$ mice suitable for comparative proteomic analysis.

High-resolution mass spectrometry has already been proven to be a powerful tool for the accurate profiling of hundreds of proteins through density gradient fractions in order to reliably identify true resident proteins of an organelle against a high background of co-purifying components [47,58,59]. In this work, we established a comparative profiling strategy for a most comprehensive quantitative assessment of the matrix protein composition of low abundant kidney peroxisomes from WT and *Pex7*$^{-/-}$ mice. Profiles of approx. 980 proteins were inferred from approx. 6941 peptide signals detected in high density gradient fractions by label-free quantitative MS and MaxQuant analysis. Supervised statistical analysis using the mean peroxisomal profiles from WT and *Pex7*$^{-/-}$ gradients as reference allowed us to reliably determine a set of peroxisomal proteins with significantly altered abundance in *Pex7*$^{-/-}$ compared to WT mice. The first group of proteins were clearly present in WT while barely detectable (Agps, Phyh, Acaa1 isoform a and b) or markedly decreased (KIAA0564) in peroxisome-enriched fractions of *Pex7*$^{-/-}$ mice. In contrast, the second group consisting of the peroxisomal enzymes Far1 isoform 4, Serhl, Lonp2 and Acsl1 were strongly upregulated in *Pex7*$^{-/-}$ compared to WT mice.

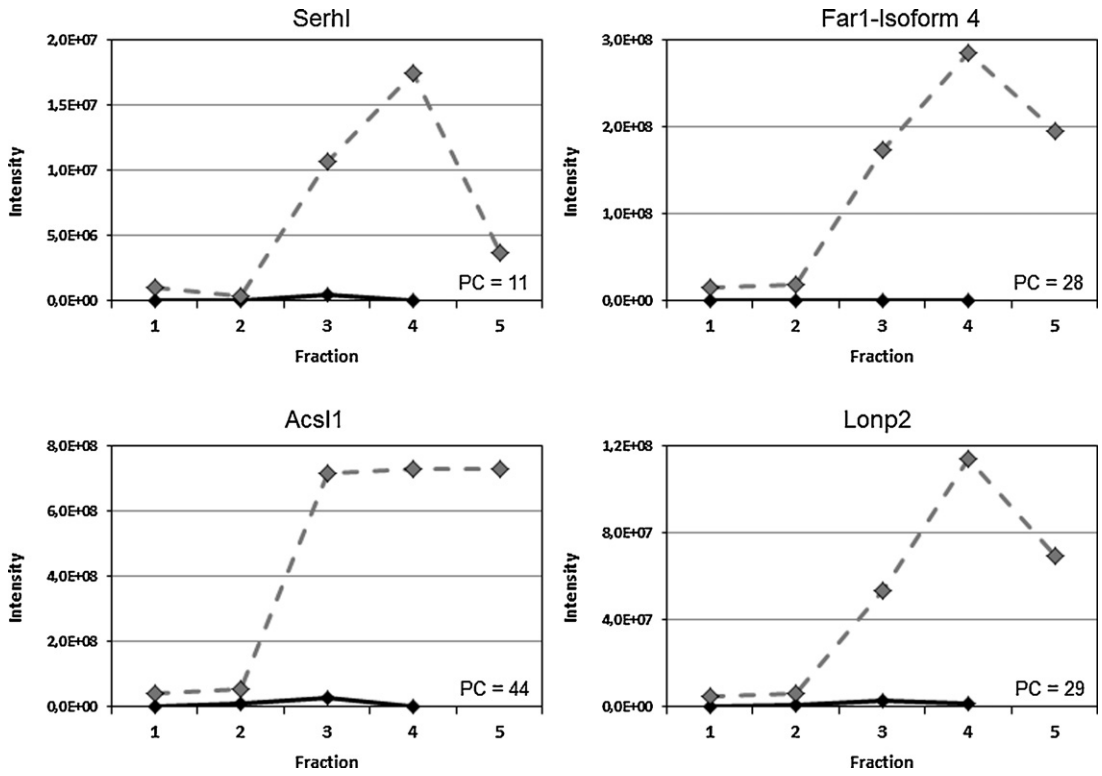

Fig. 2. Intensity profiles of serine hydrolase-like protein (Serhl), acyl CoA reductase 1 (Far1) isoform 4, long-chain acyl-Coenzyme A synthetase 1 (Acsl1), and lon protease-like protein 2 (Lonp2) in high density fractions of kidneys from wildtype (bold line) and *Pex7* knockout (dashed line) mice. PC, peptide count.

This label-free profiling approach proved to enable an in-depth study of the proteome of peroxisomes despite the presence of a high number of contaminants from other subcellular compartments. We observed differences between both the distribution and abundance of peroxisomal proteins in *Pex7*$^{-/-}$ and WT density gradients, making it more difficult to determine proteins that may only be slightly affected in abundance by the absence of Pex7. To address this limitation in future investigations and to overall increase the accuracy of label-free comparative protein profiling, distinct internal reference compounds may be used to adjust for potential variations in sample preparations. Alternatively, stable isotope labeling techniques can be employed to alleviate variations introduced by separate sample processing and, thus, to improve the sensitivity of this comparative profiling approach towards proteins exhibiting small regulation factors. In addition, adequate biological replicates would allow to study small differences in peroxisomes of WT and *Pex7*$^{-/-}$ in greater depth. However, since material of *Pex7*$^{-/-}$ mice was limiting and isolation of low-abundant peroxisomes is a challenging task in general, we followed a label-free MS-based protein profiling approach in this work, facilitating the identification of peroxisomal constituents that were significantly affected by the deletion of Pex7 as it was expected for PTS2-containing proteins.

Only a few peroxisomal enzymes are targeted to peroxisomes following specific binding of the PTS2 nonapeptide to the peroxisomal receptor Pex7. While in baker's yeast thiolase is the only protein known to exhibit a functional PTS2 [60], the peroxisomal matrix proteins Acaa1, Agps and Phyh have been characterized as PTS2 proteins in mammals [19]. Upon deletion of Pex7, the targeting of the PTS2 proteins to peroxisomes is fully prevented, while import of PTS1 proteins remains unaffected [18]. Through comparative protein profiling analysis we unequivocally identified all three currently known proteins containing a functional PTS2 as peroxisomal components that were virtually absent in *Pex7*$^{-/-}$ mice. The data thus demonstrate the feasibility of the strategy for the accurate identification of peroxisomal proteins following the Pex7 import pathway. A major benefit of the quantitative proteomics approach used here relies on monitoring organellar proteins through several consecutive gradient fractions. This comparative profiling approach promotes the possibility to identify even low abundant constituents as well as to detect drastic abundance changes of peroxisomal proteins exemplified by the known PTS2 proteins. We further obtained dependable information on the relative abundance of virtually all known PTS1-containing proteins in kidney peroxisomes from WT and *Pex7*$^{-/-}$ mice. The only exceptions were Baat, a type I acyl-CoA thioesterase involved in peroxisomal β-oxidation, the alanine-glyoxylate aminotransferase Agxt, the dehydrogenase/reductase member 2 (Dhrs2), and hydroxyl acid oxidase 1 (Hao1). Notably, the respective isoforms of the latter two enzymes, namely Dhrs4 and Hao2, were reliably monitored based on 29 and 34 unique peptide identifications indicating their specific expression in kidney. Baat was identified by a single peptide in kidney peroxisomes from WT mice only, which is consistent with previous work reporting it to be highly expressed in liver while present in vanishingly low amounts in kidney [53,57]. The import of PTS1-containing proteins was generally found to be unaffected by the deletion of the PTS2 receptor, which is in agreement with their Pex7-independent import viaPex5. However, abundance levels of Far1, Serhl, Lonp2, and Acsl1were found to be drastically increased in *Pex7*$^{-/-}$ mice, indicating that the absence of Acaa1, Agps, and Phyh causes aberrant metabolic processes in peroxisomes.

Acaa1 converts β-ketoacyl-CoA to acyl-CoA and acetyl-CoA and, thus, represents a key enzyme in the β-oxidation of VLCFAs in peroxisomes. It was therefore quite unexpected to observe that β-oxidation of VLCFAs is normal in RCDP type 1 patients [14,40,41]. In *Pex7*$^{-/-}$ mice, however, VLCFAs were found to accumulate due to impaired β-oxidation during the prenatal to early postnatal period, while β-oxidation appeared to be normal at later age [49]. Since expression of the Scp2 was found to be increased during mouse development [61], the enzyme was suggested to restore

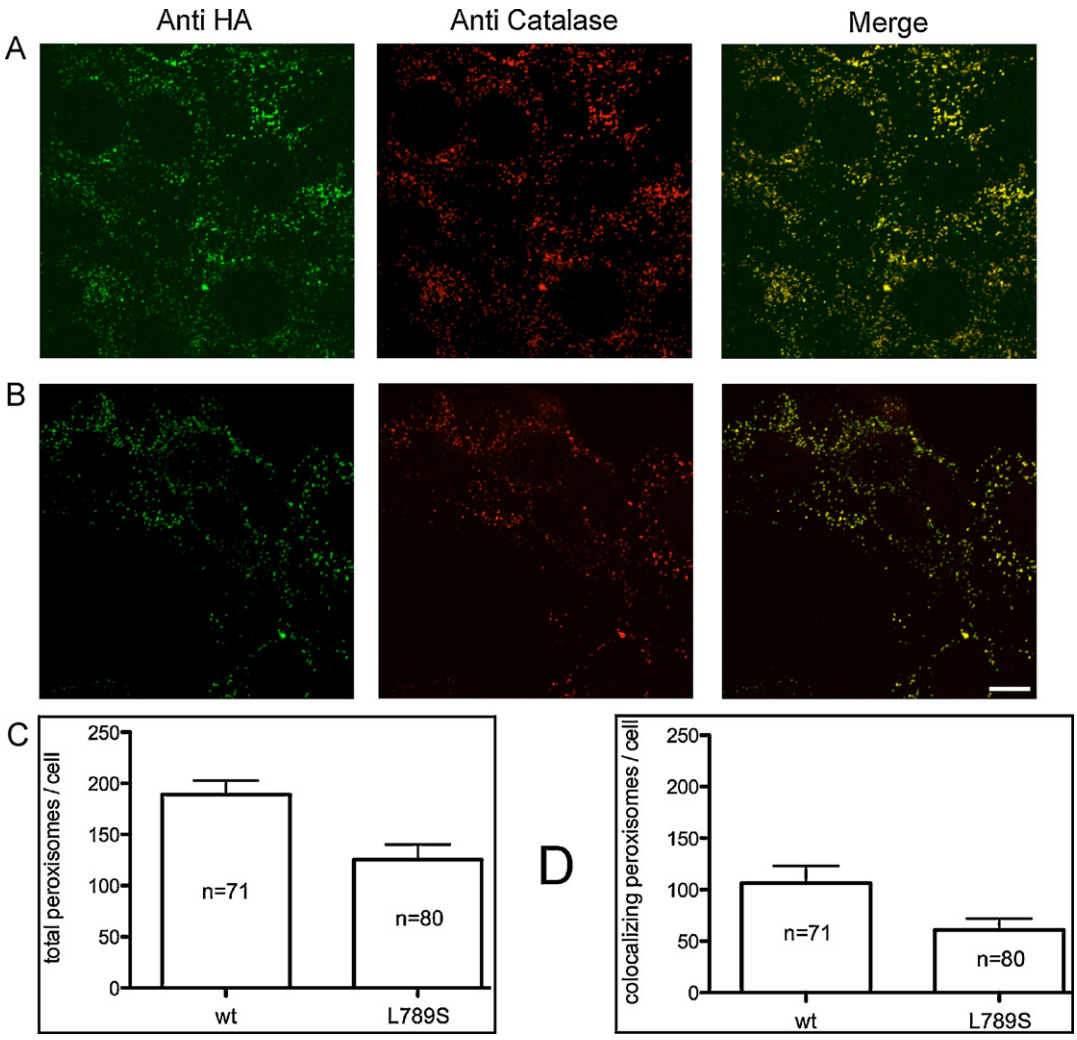

Fig. 3. Study of the intracellular localization of KIAA0564 fragments. Human hepatocellular carcinoma (Huh7) cells were stably transfected with the KIAA0564(478–939) (row A) or the KIAA0564(478–939)-L789S fragment (row B). The fragments and peroxisomes were visualized using an anti-HA and an anti-catalase primary antibody, respectively. Alexa Fluor 488 (green) and 547 (red) coupled secondary antibodies were used for staining. Images were assembled from Z-projections. The scale bar represents 10 μm. The total number of peroxisomes per cell (C) and the number of peroxisomes colocalizing with the respective KIAA0564 fragment (D) was determined by quantitative analysis of immunofluorescence images (for further details refer to text).

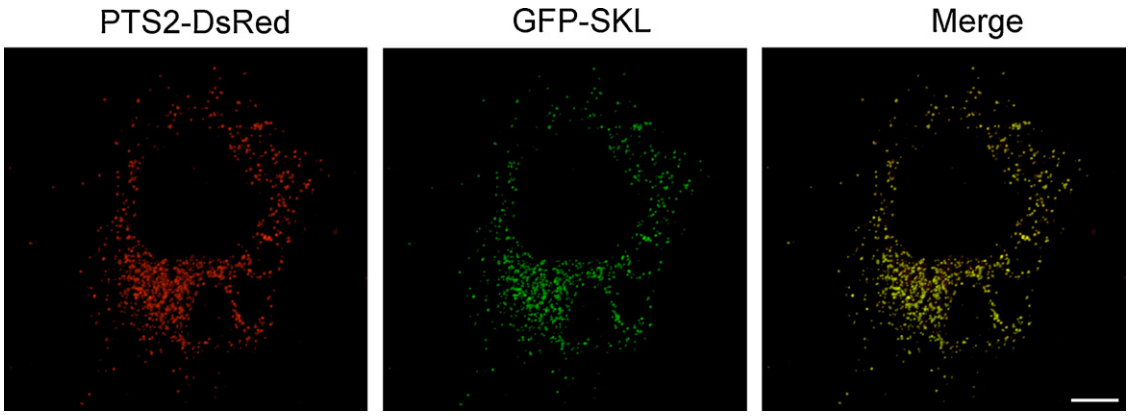

Fig. 4. Intracellular localization of the fragment KIAA0564(764–833). Shown are the fluorescence patterns of Huh7 cells transiently expressing the small putative PTS2-containing fragment KIAA0564(764–833) fused to DsRed (PTS2-DsRed) and GFP-SKL as peroxisomal marker. Images from the left to the right: KIAA0564(764–833) fragment (red), peroxisomal marker GFP-SKL (green), merge (for further details refer to text). Images were assembled from Z-projections. The scale bar represents 10 μm. (For interpretation of the references to color in this figure legend, the reader is referred to the web version of the article.)

β-oxidation at later age [49]. In agreement with this, our data indicate an increase in abundance of Scp2 in *Pex7*$^{-/-}$ while Acaa1 was nearly absent. Furthermore, Acsl1, an enzyme involved in the activation of fatty acids, was found to be considerably more abundant in *Pex7*$^{-/-}$ mice. Acox1 and Edh17b4 (better known as peroxisomal multifunctional enzyme type 2) catalyzing the first two steps in peroxisomal β-oxidation of VLCFAs were found to be moderately increased in abundance. Interestingly, levels of the acyl-CoA thioesterases Acot3, Acot6 and Acot8 were also elevated in *Pex7*$^{-/-}$ mice as well. Based on these findings it is tempting to speculate that in the absence of plasmalogens all enzymes able to generate free fatty acids and CoA, which both are substrates for the acyl-CoA synthetases, are upregulated in order to possibly maximize the rate of etherphospholipid synthesis if there is a shortage of such lipids.

Pex7$^{-/-}$ mice were previously reported to drastically accumulate phytanic acid when feeding a diet supplemented with phytol due to deficient import of Phyh being the first enzyme in the degradation of activated phytanic acid by peroxisomal α-oxidation and to exhibit a strong reduction in plasmalogens due to the absence of Agps being the first enzyme in ether-phospholipid biosynthesis [49]. Recently, activity of Far1, the peroxisomal enzyme providing long-chain alcohols for the synthesis of ether-linked alkyl bonds by Agps, was found to be significantly increased in plasmalogen-deficient cells [62]. Following the resupply of plasmalogens, the enzyme activity was restored to normal values through increased turnover of Far1. Hence, ether-phospholipid biosynthesis was suggested to be controlled by a negative feedback mechanism adjusting Far1 levels to the pool of plasmalogens present in the cell. In plasmalogen-deficient fibroblasts derived from RCDP patients, the activity of Far1 was found to be markedly increased as well [63]. Consistent with these reports, we determined a considerable increase in the abundance of Far1while the abundance of Agps was fully diminished in *Pex7*$^{-/-}$ mice.

Through comparative profiling we further discovered strongly increased abundance levels of the peroxisomal enzymes Serhl and Lonp2. Although the Serhl gene is conserved in human, dog, cow, rat/mouse, chicken, zebrafish, fruit fly, and mosquito, there is currently no information about the potential function of this 35 kDa protein. The enzyme harbors a C-terminal PTS1 (ARL) and a serine lipase active center and has been detected in mouse kidney peroxisomes before [47]. The peroxisome-specific isoform of Lon protease, Lonp2, contains a C-terminal PTS1 (SKL) and was first identified in rat liver peroxisomes by a proteomics approach [43]. In a consecutive study, the protease was reported to likely interact with different enzymes of the peroxisomal β-oxidation and was suggested to control the activity as well as the sorting and processing of PTS1- but not PTS2-containing peroxisomal enzymes [64]. In addition, evidence was provided that Lonp2 plays a role in peroxisome morphology [64,65] or degradation [66]. Based on our findings we suggest that increased abundance of Lonp2 in *Pex7*$^{-/-}$ mice ensures proper sorting and processing of PTS1-containing enzymes involved in peroxisomal β-oxidation that were found to exhibit increased activity levels as a consequence of impaired import of Acaa1 into peroxisomes.

Comparative profiling of high density gradient fractions of WT and *Pex7*$^{-/-}$ mice revealed the near absence of all the three known functional PTS2 proteins and a more than 5-fold reduction of KIAA0564, a so far uncharacterized protein, in peroxisomal fractions of *Pex7*$^{-/-}$ mice. The KIAA0564 gene is well conserved across species and mouse KIAA0564 exhibits 86% sequence identity to its human homologue containing a putative PTS2 (KIVDRFLHL at aa 781–789) according to PSORT [54]. The PTS2 is generally defined as a nonapeptide exhibiting the consensus sequence (R/K)(L/V/I)X_5(H/Q)(L/A) with X being any amino acid. Mutations in the first and last two amino acids of this consensus sequence have been shown to lead to aberrant targeting of PTS2 proteins [18]. Apart from this, two further PTS2 consensus sequences, R(L/V/I/Q)XX(L/V/I/H)(L/S/G/A)X(H/Q)(L/A)and (R/K)(L/V/I/Q)XX(L/V/I/H/Q)(L/S/G/A/K)X(H/Q)(L/A/F), have been reported by taking into account the main variants or most common variants of the PTS2 sequence [67]. In addition, functional PTS2 sequences are typically located at the N-terminal end, although they have also been reported to be functional in the middle or at the C-terminus of a protein [23].

In this work, we observed KIAA0564(478–939) and KIAA0564(478–939)-L789S fragments in punctate structures that corresponded well to the pattern of catalase, pointing to their peroxisomal localization. As a consequence of the L789S mutation replacing the basic amino acid at position #9 of the PTS2 sequence by serine, we expected impaired targeting; however, we found only a slight effect on the number of colocalizing substructures, whereas the average number of peroxisomes in Huh7 cells expressing the mutated fragment compared to the WT fragment was increased by more than 30%. Interestingly, when expressing only a short, the putative PTS2 containing fragment of 69 amino acids (aa 764–833) as DsRed fusion construct we found this small fragment in punctate structures that colocalized with peroxisomes, which in turn points to the presence of a functional PTS2 and, thus, provides the first evidence that KIAA0564 is indeed imported into peroxisomes via the PTS2 pathway.

5. Conclusions

Comparative MS-based proteome profiling as reported here proved to be an effective tool for identifying proteins specifically affected by the deletion of Pex7. The virtual absence of all known PTS2 proteins in *Pex7*$^{-/-}$ mice was unequivocally shown, demonstrating the high potential of this strategy for pinpointing proteins following the Pex7 import pathway. The approach is unbiased and does not rely on a priori information about putative PTS2 sequences or peroxisomal localization of proteins. It is further expected to be equally well applicable to other species and to effectively complement bioinformatics approaches for identifying mammalian PTS2 proteins that have been of limited success so far. Moreover, information about changes in the abundance of PTS1 proteins further assists in eventually gaining a comprehensive understanding of impaired peroxisome function caused by the malfunctioning or absence of Pex7.

Acknowledgements

The authors would like to thank Nadine Stoepel for excellent technical assistance. We are grateful to Prof. Nils Johnsson (Ulm University) for scientific support and Dr. Silke Oeljeklaus for critically reading the manuscript. This work was supported by the FP6 European Union Project “Peroxisome” (LSHG-CT-2004-512018) as well as by the Deutsche Forschungsgemeinschaft and the Excellence Initiative of the German Federal and State Governments (EXC 294 BIOSS).

Appendix A. Supplementary data

Supplementary data associated with this article can be found, in the online version, at doi:10.1016/j.ijms.2011.09.005.

References

[1] T.C. Walther, M. Mann, Mass spectrometry-based proteomics in cell biology, J. Cell Biol. 190 (2010) 491–500.
[2] E. Wiederhold, L.M. Veenhoff, B. Poolman, D.J. Slotboom, Proteomics of *Saccharomyces cerevisiae* organelles, Mol. Cell. Proteomics 9 (2010) 431–445.
[3] C.E. Au, A.W. Bell, A. Gilchrist, J. Hiding, T. Nilsson, J.J. Bergeron, Organellar proteomics to create the cell map, Curr. Opin. Cell Biol. 19 (2007) 376–385.

[4] J.S. Andersen, M. Mann, Organellar proteomics: turning inventories into insights, EMBO Rep. 7 (2006) 874–879.
[5] J.R. Yates III, A. Gilchrist, K.E. Howell, J.J.M. Bergeron, Proteomics of organelles and large cellular structures, Nat. Rev. Mol. Cell Biol. 6 (2005) 702–714.
[6] M. Dreger, Subcellular proteomics, Mass Spectrom. Rev. 22 (2003) 27–56.
[7] R. Saleem, J. Smith, J. Aitchison, Proteomics of the peroxisome, Biochim. Biophys. Acta: Mol. Cell Res. 1763 (2006) 1541–1551.
[8] R.J.A. Wanders, H.R. Waterham, Peroxisomal disorders: the single peroxisomal enzyme deficiencies, Biochim. Biophys. Acta: Mol. Cell Res. 1763 (2006) 1707–1720.
[9] Y. Fujiki, Peroxisome biogenesis and peroxisome biogenesis disorders, FEBS Lett. 476 (2000) 42–46.
[10] S.J. Gould, D. Valle, Peroxisome biogenesis disorders: genetics and cell biology, Trends Genet. 16 (2000) 340–345.
[11] P.E. Purdue, J.W. Zhang, M. Skoneczny, P.B. Lazarow, Rhizomelic chondrodysplasia punctata is caused by deficiency of human PEX7, a homologue of the yeast PTS2 receptor, Nat. Genet. 15 (1997) 381–384.
[12] A.M. Motley, E.H. Hettema, E.M. Hogenhout, P. Brites, A.L. ten Asbroek, F.A. Wijburg, F. Baas, H.S. Heijmans, H.F. Tabak, R.J.A. Wanders, B. Distel, Rhizomelic chondrodysplasia punctata is a peroxisomal protein targeting disease caused by a non-functional PTS2 receptor, Nat. Genet. 15 (1997) 377–380.
[13] N. Braverman, G. Steel, C. Obie, A. Moser, H. Moser, S.J. Gould, D. Valle, Human PEX7 encodes the peroxisomal PTS2 receptor and is responsible for rhizomelic chondrodysplasia punctata, Nat. Genet. 15 (1997) 369–376.
[14] H.S. Heymans, J.W. Oorthuys, G. Nelck, R.J.A. Wanders, R.B. Schutgens, Rhizomelic chondrodysplasia punctata: another peroxisomal disorder, N. Engl. J. Med. 313 (1985) 187–188.
[15] J.W. Zhang, P.B. Lazarow, Peb1p (Pas7p) is an intraperoxisomal receptor for the NH2-terminal, type 2, peroxisomal targeting sequence of thiolase: Peb1p itself is targeted to peroxisomes by an NH2-terminal peptide, J. Cell Biol. 132 (1996) 325–334.
[16] P. Rehling, M. Marzioch, F. Niesen, E. Wittke, M. Veenhuis, W.H. Kunau, The import receptor for the peroxisomal targeting signal 2 (PTS2) in *Saccharomyces cerevisiae* is encoded by the PAS7 gene, EMBO J. 15 (1996) 2901–2913.
[17] K. Ghys, M. Fransen, G.P. Mannaerts, P.P. van Veldhoven, Functional studies on human Pex7p: subcellular localization and interaction with proteins containing a peroxisome-targeting signal type 2 and other peroxins, Biochem. J. 365 (2002) 41–50.
[18] P. Lazarow, The import receptor Pex7p and the PTS2 targeting sequence, Biochim. Biophys. Acta: Mol. Cell Res. 1763 (2006) 1599–1604 (Chapter 3.1.7).
[19] R.J.A. Wanders, H.R. Waterham, Biochemistry of mammalian peroxisomes revisited, Annu. Rev. Biochem. 75 (2006) 295–332.
[20] J. Wolf, W. Schliebs, R. Erdmann, Peroxisomes as dynamic organelles: peroxisomal matrix protein import, FEBS J. 277 (2010) 3268–3278.
[21] C. Brocard, A. Hartig, Peroxisome targeting signal 1: is it really a simple tripeptide? Biochim. Biophys. Acta: Mol. Cell Res. 1763 (2006) 1565–1573.
[22] S.J. Gould, G.A. Keller, N. Hosken, J. Wilkinson, S. Subramani, A conserved tripeptide sorts proteins to peroxisomes, J. Cell Biol. 108 (1989) 1657–1664.
[23] J.E. Legakis, S.R. Terlecky, PTS2 protein import into mammalian peroxisomes, Traffic 2 (2001) 252–260.
[24] B.W. Swinkels, S.J. Gould, A.G. Bodnar, R.A. Rachubinski, S. Subramani, A novel, cleavable peroxisomal targeting signal at the amino-terminus of the rat 3-ketoacyl-CoA thiolase, EMBO J. 10 (1991) 3255–3262.
[25] T. Tsukamoto, S. Hata, S. Yokota, S. Miura, Y. Fujiki, M. Hijikata, S. Miyazawa, T. Hashimoto, T. Osumi, Characterization of the signal peptide at the amino terminus of the rat peroxisomal 3-ketoacyl-CoA thiolase precursor, J. Biol. Chem. 269 (1994) 6001–6010.
[26] H. Otera, T. Harano, M. Honsho, K. Ghaedi, S. Mukai, A. Tanaka, A. Kawai, N. Shimizu, Y. Fujiki, The mammalian peroxin Pex5pL, the longer isoform of the mobile peroxisome targeting signal (PTS) type 1 transporter, translocates the Pex7p.PTS2 protein complex into peroxisomes via its initial docking site, Pex14p, J. Biol. Chem. 275 (2000) 21703–21714.
[27] T. Matsumura, H. Otera, Y. Fujiki, Disruption of the interaction of the longer isoform of Pex5p, Pex5pL, with Pex7p abolishes peroxisome targeting signal type 2 protein import in mammals. Study with a novel Pex5-impaired Chinese hamster ovary cell mutant, J. Biol. Chem. 275 (2000) 21715–21721.
[28] N. Braverman, G. Dodt, S.J. Gould, D. Valle, An isoform of pex5p, the human PTS1 receptor, is required for the import of PTS2 proteins into peroxisomes, Hum. Mol. Genet. 7 (1998) 1195–1205.
[29] N. Braverman, L. Chen, P. Lin, C. Obie, G. Steel, P. Douglas, P.K. Chakraborty, J.T.R. Clarke, A. Boneh, A. Moser, H. Moser, D. Valle, Mutation analysis of PEX7 in 60 probands with rhizomelic chondrodysplasia punctata and functional correlations of genotype with phenotype, Hum. Mutat. 20 (2002) 284–297.
[30] A.M. Motley, P. Brites, L. Gerez, E. Hogenhout, J. Haasjes, R. Benne, H.F. Tabak, R.J.A. Wanders, H.R. Waterham, Mutational spectrum in the PEX7 gene and functional analysis of mutant alleles in 78 patients with rhizomelic chondrodysplasia punctata type 1, Am. J. Hum. Genet. 70 (2002) 612–624.
[31] N. Shimozawa, Y. Suzuki, Z. Zhang, A. Imamura, R. Toyama, S. Mukai, Y. Fujiki, T. Tsukamoto, T. Osumi, T. Orii, R.J.A. Wanders, N. Kondo, Nonsense and temperature-sensitive mutations in PEX13 are the cause of complementation group H of peroxisome biogenesis disorders, Hum. Mol. Genet. 8 (1999) 1077–1083.
[32] A. Bout, Y. Teunissen, T. Hashimoto, R. Benne, J.M. Tager, Nucleotide sequence of human peroxisomal 3-oxoacyl-CoA thiolase, Nucleic Acids Res. 16 (1988) 10369.
[33] E.C. de Vet, H. van den Bosch, Alkyl-dihydroxyacetonephosphate synthase, Cell Biochem. Biophys. 32 (Spring) (2000) 117–121.
[34] G.A. Jansen, E.M. Hogenhout, S. Ferdinandusse, H.R. Waterham, R. Ofman, C. Jakobs, O.H. Skjeldal, R.J.A. Wanders, Human phytanoyl-CoA hydroxylase: resolution of the gene structure and the molecular basis of Refsum's disease, Hum. Mol. Genet. 9 (2000) 1195–1200.
[35] S.J. Mihalik, J.C. Morrell, D. Kim, K.A. Sacksteder, P.A. Watkins, S.J. Gould, Identification of PAHX, a Refsum disease gene, Nat. Genet. 17 (1997) 185–189.
[36] G.A. Jansen, R. Ofman, S. Ferdinandusse, L. Ijlst, A.O. Muijsers, O.H. Skjeldal, O. Stokke, C. Jakobs, G.T. Besley, J.E. Wraith, R.J.A. Wanders, Refsum disease is caused by mutations in the phytanoyl-CoA hydroxylase gene, Nat. Genet. 17 (1997) 190–193.
[37] R.J.A. Wanders, W. Smit, H.S. Heymans, R.B. Schutgens, P.G. Barth, H. Schierbeek, G.P. Smit, R. Berger, H. Przyrembel, T.A. Eggelte, Age-related accumulation of phytanic acid in plasma from patients with the cerebro-hepato-renal (Zellweger) syndrome, Clin. Chim. Acta 166 (1987) 45–56.
[38] E.C. de Vet, L. Ijlst, W. Oostheim, R.J.A. Wanders, H. van den Bosch, Alkyl-dihydroxyacetonephosphate synthase. Fate in peroxisome biogenesis disorders and identification of the point mutation underlying a single enzyme deficiency, J. Biol. Chem. 273 (1998) 10296–10301.
[39] E.C. de Vet, L. Ijlst, W. Oostheim, C. Dekker, H.W. Moser, H. van den Bosch, R.J.A. Wanders, Ether lipid biosynthesis: alkyl-dihydroxyacetonephosphate synthase protein deficiency leads to reduced dihydroxyacetonephosphate acyltransferase activities, J. Lipid Res. 40 (1999) 1998–2003.
[40] G. Hoefler, S. Hoefler, P.A. Watkins, W.W. Chen, A. Moser, V. Baldwin, B. McGillivary, J. Charrow, J.M. Friedman, L. Rutledge, Biochemical abnormalities in rhizomelic chondrodysplasia punctata, J. Pediatr. 112 (1988) 726–733.
[41] P.E. Purdue, M. Skoneczny, X. Yang, J.W. Zhang, P.B. Lazarow, Rhizomelic chondrodysplasia punctata, a peroxisomal biogenesis disorder caused by defects in Pex7p, a peroxisomal protein import receptor: a minireview, Neurochem. Res. 24 (1999) 581–586.
[42] M. Islinger, M.J.R. Cardoso, M. Schrader, Be different—the diversity of peroxisomes in the animal kingdom, Biochim. Biophys. Acta 1803 (2010) 881–897.
[43] M. Kikuchi, N. Hatano, S. Yokota, N. Shimozawa, T. Imanaka, H. Taniguchi, Proteomic analysis of rat liver peroxisome: presence of peroxisome-specific isozyme of Lon protease, J. Biol. Chem. 279 (2004) 421–428.
[44] M. Islinger, G.H. Lüers, H. Zischka, M. Ueffing, A. Völkl, Insights into the membrane proteome of rat liver peroxisomes: microsomal glutathione-S-transferase is shared by both subcellular compartments, Proteomics 6 (2006) 804–816.
[45] R. Ofman, D. Speijer, R. Leen, R.J.A. Wanders, Proteomic analysis of mouse kidney peroxisomes: identification of RP2p as a peroxisomal nudix hydrolase with acyl-CoA diphosphatase activity, Biochem. J. 393 (2006) 537–543.
[46] M. Islinger, G.H. Lüers, K.W. Li, M. Loos, A. Völkl, Rat liver peroxisomes after fibrate treatment. A survey using quantitative mass spectrometry, J. Biol. Chem. 282 (2007) 23055–23069.
[47] S. Wiese, T. Gronemeyer, R. Ofman, M. Kunze, C.P. Grou, J.A. Almeida, M. Eisenacher, C. Stephan, H. Hayen, L. Schollenberger, T. Korosec, H.R. Waterham, W. Schliebs, R. Erdmann, J. Berger, H.E. Meyer, W. Just, J.E. Azevedo, R.J.A. Wanders, B. Warscheid, Proteomics characterization of mouse kidney peroxisomes by tandem mass spectrometry and protein correlation profiling, Mol. Cell. Proteomics 6 (2007) 2045–2057.
[48] A. Schlüter, A. Real-Chicharro, T. Gabaldón, F. Sánchez-Jiménez, A. Pujol, PeroxisomeDB 2.0: an integrative view of the global peroxisomal metabolome, Nucleic Acids Res. 38 (2010) D800–D805.
[49] P. Brites, A.M. Motley, P. Gressens, P.A.W. Mooyer, I. Ploegaert, V. Everts, P. Evrard, P. Carmeliet, M. Dewerchin, L. Schoonjans, M. Duran, H.R. Waterham, R.J.A. Wanders, M. Baes, Impaired neuronal migration and endochondral ossification in Pex7 knockout mice: a model for rhizomelic chondrodysplasia punctata, Hum. Mol. Genet. 12 (2003) 2255–2267.
[50] R.J.A. Wanders, C.W. van Roermund, D.S. Schor, H.J. ten Brink, C. Jakobs, 2-Hydroxyphytanic acid oxidase activity in rat and human liver and its deficiency in the Zellweger syndrome, Biochim. Biophys. Acta 1227 (1994) 177–182.
[51] M. Kaller, S.-T. Liffers, S. Oeljeklaus, K. Kuhlmann, S. Röh, R. Hoffmann, B. Warscheid, H. Hermeking, Genome-wide characterization of miR-34a induced changes in protein and mRNA expression by a combined pulsed SILAC and micro-array analysis, Mol. Cell. Proteomics 10 (August (8)) (2011), M111.010462.
[52] J. Cox, N. Neuhauser, A. Michalski, R.A. Scheltema, J.V. Olsen, M. Mann, Andromeda: a peptide search engine integrated into the MaxQuant environment, J. Proteome Res. 10 (2011) 1794–1805.
[53] B.J. Woodcroft, L. Hammond, J.L. Stow, N.A. Hamilton, Automated organelle-based colocalization in whole-cell imaging, Cytometry A 75 (2009) 941–950.
[54] K. Nakai, P. Horton, PSORT: a program for detecting sorting signals in proteins and predicting their subcellular localization, Trends Biochem. Sci. 24 (1999) 34–36.
[55] M. Islinger, K.W. Li, J. Seitz, A. Völkl, G.H. Lüers, Hitchhiking of Cu/Zn superoxide dismutase to peroxisomes—evidence for a natural piggyback import mechanism in mammals, Traffic 10 (2009) 1711–1721.
[56] K.A. Sacksteder, J.M. Jones, S.T. South, X. Li, Y. Liu, S.J. Gould, PEX19 binds multiple peroxisomal membrane proteins, is predominantly cytoplasmic, and is required for peroxisome membrane synthesis, J. Cell Biol. 148 (2000) 931–944.
[57] K. Solaas, B.F. Kase, V. Pham, K. Bamberg, M.C. Hunt, S.E. Alexson, Differential regulation of cytosolic and peroxisomal bile acid amidation by PPAR activation favors the formation of unconjugated bile acids, J. Lipid Res. 45 (2004) 1051–1060.

[58] L.J. Foster, C.L. de Hoog, Y. Zhang, Y. Zhang, X. Xie, V.K. Mootha, M. Mann, A mammalian organelle map by protein correlation profiling, Cell 125 (2006) 187–199.
[59] J.S. Andersen, C.J. Wilkinson, T. Mayor, P. Mortensen, E.A. Nigg, M. Mann, Proteomic characterization of the human centrosome by protein correlation profiling, Nature 426 (2003) 570–574.
[60] S. Grunau, W. Schliebs, R. Linnepe, C. Neufeld, C. Cizmowski, B. Reinartz, H.E. Meyer, B. Warscheid, W. Girzalsky, R. Erdmann, Peroxisomal targeting of PTS2 pre-import complexes in the yeast *Saccharomyces cerevisiae*, Traffic 10 (2009) 451–460.
[61] S. Huyghe, M. Casteels, A. Janssen, L. Meulders, G.P. Mannaerts, P.E. Declercq, P.P. van Veldhoven, M. Baes, Prenatal and postnatal development of peroxisomal lipid-metabolizing pathways in the mouse, Biochem. J. 353 (2001) 673–680.
[62] M. Honsho, S. Asaoku, Y. Fujiki, Posttranslational regulation of fatty acyl-CoA reductase 1, Far1, controls ether glycerophospholipid synthesis, J. Biol. Chem. 285 (2010) 8537–8542.
[63] W.B. Rizzo, D.A. Craft, L.L. Judd, H.W. Moser, A.B. Moser, Fatty alcohol accumulation in the autosomal recessive form of rhizomelic chondrodysplasia punctata, Biochem. Med. Metab. Biol. 50 (1993) 93–102.
[64] S. Omi, R. Nakata, K. Okamura-Ikeda, H. Konishi, H. Taniguchi, Contribution of peroxisome-specific isoform of Lon protease in sorting PTS1 proteins to peroxisomes, J. Biochem. 143 (2008) 649–660.
[65] E.B. Aksam, A. Koek, J.A.K.W. Kiel, S. Jourdan, M. Veenhuis, I.J. van der Klei, A peroxisomal lon protease and peroxisome degradation by autophagy play key roles in vitality of Hansenula polymorpha cells, Autophagy 3 (2007) 96–105.
[66] S. Yokota, H. Dariush Fahimi, Degradation of excess peroxisomes in mammalian liver cells by autophagy and other mechanisms, Histochem. Cell Biol. 131 (2009) 455–458.
[67] O.I. Petriv, L. Tang, V.I. Titorenko, R.A. Rachubinski, A new definition for the consensus sequence of the peroxisome targeting signal type 2, J. Mol. Biol. 341 (2004) 119–134.